ELSEVIER

Polymer 44 (2003) 2883–2889

polymer

www.elsevier.com/locate/polymer

Detailed studies of the initiation step in free radical polymerization of α-(substituted methyl)acrylates by electron paramagnetic resonance spectroscopy

Eriko Sato, Per B. Zetterlund, Bunichiro Yamada*

Department of Applied and Bioapplied Chemistry, Graduate School of Engineering, Osaka City University, Osaka 558-8585, Japan

Received 24 December 2002; received in revised form 20 February 2003; accepted 21 February 2003

Abstract

Reactions of the adduct radical obtained by addition of the initiator-derived 2-carbomethoxy-2-propyl radical to methyl α-[(2-methyl-2-carbomethoxy)propyl]acrylate (the unsaturated dimer of methyl methacrylate (MMAD)) have been monitored by electron paramagnetic resonance spectroscopy. Rate constants for addition of the 2-carbomethoxy-2-propyl radical to MMAD, mutual reactions between the adduct radicals, and reactions of the adduct radical and the 2-carbomethoxy-2-propyl radical, and β-fragmentation of the adduct radical were evaluated by steady-state and non-steady-state kinetic analysis in tandem with computer modeling and simulations involving parameter optimization procedures. The resulting rate constants showed that addition and radical–radical reactions between low molecular weight radicals are suppressed due to the marked steric congestion of the carbon-carbon double bond and radical center, respectively, and that β-fragmentation can compete with radical–radical reactions of the adduct radicals depending on the radical concentration.

Keywords: EPR spectroscopy; β-Fragmentation; Steric hindrance

1. Introduction

α-(Substituted methyl)acrylates show versatile free radical polymerization behavior as homopolymerizable monomers, addition-fragmentation chain transfer (AFCT) agents, and polymerizable AFCT agents [1,2]. Some of them, e.g. methyl α-[2,2-bis(carbomethoxy)ethyl]acrylate (M(DM)EA) [3] and methyl α-(2-carbomethoxyethyl)acrylate (MMEA) [4,5], homopolymerize readily to high molecular weight despite bearing bulky α-substituents.

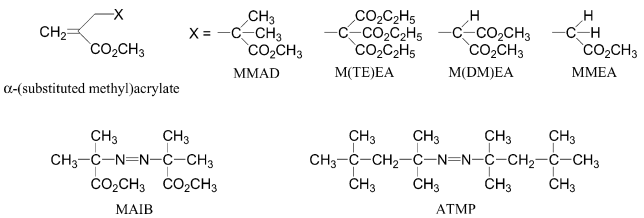

This polymerization behavior is known as Steric Hindrance Assisted Polymerization (SHAP), and is characterized by a favorable balance between slow propagation and termination rates due to steric hindrance of the α-substituents. Primary propagating radicals (PPRs) of polymerizable monomers normally add rapidly to monomer, thus making it difficult to study the initiation step under ordinary polymerization conditions. However, the PPRs generated by addition of primary radical from initiator (PRI) to certain vinyl compounds have been detected by electron paramagnetic resonance (EPR) spectroscopy; e.g. di-*n*-butyl itaconates [6], *tert*-butyl α-(*tert*-butylsulfenyl)acrylate [7], α-(*tert*-butylsulfenyl)acrylonitrile [8], α-(ethylsulfenyl)acrylonitrile [9], methyl phenylethyl itaconate (above the ceiling temperature) [10], methyl α-[(2-methyl-2-carbomethoxy)propyl]acrylate [11,12] (the unsaturated dimer of methyl methacrylate (MMAD), and the α-(substituted methyl) acrylate functioning as an AFCT agent), and methyl α-[2,2,2-tris(carbethoxy)ethyl]acrylate (M(TE)EA) [13]. Tanaka et al. [12] managed to detect PPR from MMAD and the 2-carbomethoxy-2-propyl radical by EPR spectroscopy to show the persistency of the adduct radical.

* Corresponding author. Tel./fax: +81-6-6605-2797.
E-mail address: yamada@a-chem.eng.osaka-cu.ac.jp (B. Yamada).

0032-3861/03/$ - see front matter © 2003 Elsevier Science Ltd. All rights reserved.
doi:10.1016/S0032-3861(03)00183-6

MMAD provides an opportunity to investigate the formation and reactions of PPR, which can be regarded as a part of the initiation step in free radical polymerization.

When a photoinitiator is employed, initiation can be instantaneously controlled by switching on and off the irradiation of light of the appropriate wavelength, and the pre-effect, steady-state and after-effect can be observed [14]. The decay of PPR from M(TE)EA and 2,4,4-trimethyl-2-pentyl radical during the after-effect has been observed by EPR spectroscopy, and it was shown that PPR is consumed by radical–radical reaction with a rate constant close to 1.3×10^3 L mol^{-1} s^{-1} at 60 °C [13]. In our previous paper [15], we showed employing the nitroxide trapping technique that the PPR from MMAD and the *tert*-butoxy radical undergoes β-fragmentation and expels the 2-carbomethoxy-2-propyl radical. Under the conditions of the nitroxide trapping experiments, alkoxyamines that could result from further reactions of the expelled radical were not detected because of the presence of an excess amount of nitroxide trapping agent. However, under the experimental conditions of EPR measurements, it was expected that the expelled radicals would be involved in further reactions such as radical–radical reactions and addition to monomer.

In this study, the reaction of the 2-carbomethoxy-2-propyl radical (generated by photolysis of initiator and fragmentation of the PPR) with MMAD, and further reactions involving the PPR and the expelled radical have been investigated by EPR spectroscopy. The rate constants for addition of PRI to MMAD, for the two types of radical–radical reactions involving PPR and the expelled radical (and PRI), and for β-fragmentation of PPR were estimated by extensive kinetic analysis involving computer simulations and parameter optimization procedures. The results are discussed in terms of steric hindrance of the α-substituent.

2. Experimental

2.1. Materials

MMAD was prepared by dimerization of MMA [16] and was distilled under reduced pressure before use. Commercially available dimethyl 2,2′-azobis(2-methylpropionate) (Wako) (MAIB) was recrystallized from *n*-hexane. 2,2′-Azobis(2,2,4-trimethylpentane) (Wako) (ATMP) was distilled under reduced pressure. Commercially available 2,2,6,6-tetramethylpiperidynyl-1-oxyl (Aldrich) (TEMPO = T) was purified by sublimation. Solvents were purified by conventional methods.

2.2. EPR measurements

EPR spectra were recorded in benzene using a Bruker ESP-300 spectrometer at X band with 100 kHz field modulation at a microwave power of 2 mW and a modulation amplitude of 0.5 G. The spectrum was recorded during 10 scans over a magnetic field width of 70 G divided into 1024 data points, and both the conversion time and the time constant were 40.96 ms. The reaction mixture was contained in a 5 mm o.d. quartz tube sealed under vacuum. A xenon lamp (1 kW) was used as the UV light source at a distance of approximately 45 cm from the EPR tube. For measurement of radical concentration within short time intervals during the pre-effect (including the steady-state) and the after-effect, the spectral intensity was recorded at the fixed magnetic field where the largest peak appeared. It was confirmed that this peak height is proportional to the double integral of the full spectrum. Absolute radical concentrations were determined based on the linear relationship between the double integral of the EPR spectrum and known concentrations of TEMPO in benzene.

2.3. Determination of $k_d f$

The value of $k_d f$ for MAIB during UV irradiation was measured by a scavenger method employing T, assuming that the PRIs of MAIB escaping the solvent cage are quantitatively trapped by TEMPO as expressed in Eq. (1):

$$-\frac{\mathrm{d[T]}}{\mathrm{d}t} = R_\mathrm{i} = 2k_\mathrm{d} f[\mathrm{I}] \tag{1}$$

where f, k_d and I denote the initiator efficiency, the rate constant for decomposition of initiator, and initiator, respectively. The concentration of TEMPO as a function of time is shown in Fig. 1, where the rate of PRI formation (R_i) is given by the slope of the linear plot. The value of $k_d f$ was determined to be 3.8×10^{-5} s^{-1} under UV irradiation at 30 °C.

2.4. Simulations

Simulations and parameter optimization procedures were performed employing the commercially available software package VisSim 2.0j. Simulations were carried out by

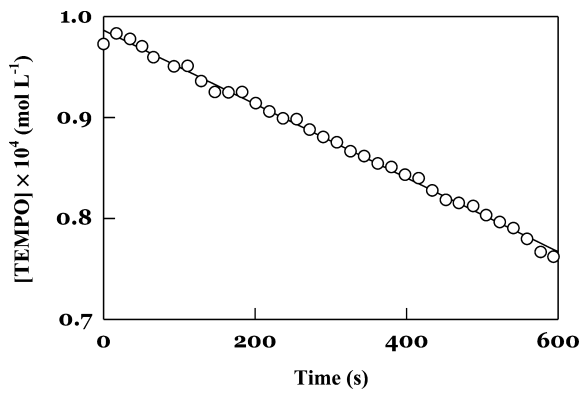

Fig. 1. Consumption of TEMPO by the reaction with PRI from MAIB under UV irradiation at 30 °C in benzene: [MAIB] = 4.90×10^{-4} mol L^{-1} and [TEMPO] = 9.98×10^{-4} mol L^{-1}.

numerical integration using the Runge Kutta 4th order algorithm. Several different sets of initial values were used as input for the unknown parameters in the non-linear least-squares optimization procedures to ensure that the global minima were found in all cases.

3. Results and discussion

The reactions expected during photolysis of MAIB in the presence of MMAD, including the reactions of the radicals expelled by fragmentation of adduct radicals, are shown and rate constants for the respective reactions are as follows:

$$I \xrightarrow{k_d} 2R^{\cdot}$$

$$R^{\cdot} + M \xrightarrow{k_{M1}} RM^{\cdot}$$

$$2RM^{\cdot} \xrightarrow{k_{t1}} P_1$$

$$RM^{\cdot} + R^{\cdot} \xrightarrow{k_{t2}} P_2$$

$$2R^{\cdot} \xrightarrow{k_{t3}} P_3$$

$$RM^{\cdot} \xrightarrow{k_{\beta}} M + R^{\cdot}$$

where I, M, $R^{\cdot}$, and $RM^{\cdot}$ represent MAIB, MMAD, the 2-carbomethoxy-2-propyl radical and PPR, respectively. P_1, P_2 and P_3 denote products from radical–radical reactions. Although MMAD may be generated via reactions of $R^{\cdot}$, this will have a negligible effect on the MMAD concentration and thus was not included in the kinetic analysis [17].

Figs. 2(a) and (b) show the EPR spectra observed during the reaction of MMAD and the 2-carbomethoxy-2-propyl radical to form PPR at 30 °C under UV irradiation (Scheme 1), and 180 s after UV interruption, respectively. The hyperfine splitting of the spectra can be explained by coupling of the two sets of two β-methylene protons and the methoxy protons of PPR (**1**): $a_{\beta-H} = 11.7$ and $a_{OMe} = 1.2$ G. The concentration of **1** during the pre-effect, steady-state

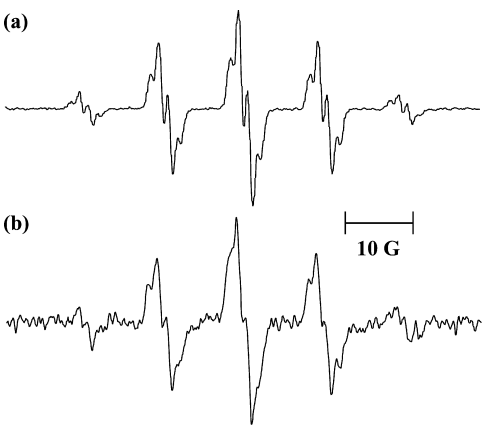

Fig. 2. EPR spectrum of the PPR observed during UV irradiation (a) and after 180 s UV interruption (b): [MMAD] = 1.0 mol L^{-1} and [MAIB] = 0.28 mol L^{-1} in benzene at 30 °C.

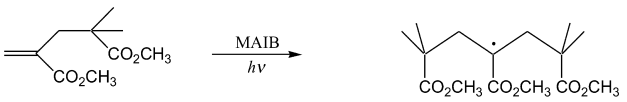

1

Scheme 1.

and after-effect is obtained and will be discussed later (Fig. 6 as a full line).

3.1. Estimation of k_{t1}

3.1.1. Effect of temperature

The decay of the PPR after interruption of UV irradiation at 30 °C is shown in Fig. 3(a) as a full line. If only radical–radical reaction of PPRs occurred, the consumption rate would be described by Eq. (2),

$$-\frac{d[RM^{\cdot}]}{dt} = k_{t1}[RM^{\cdot}]^2 \quad (2)$$

where $[RM^{\cdot}]$ and k_{t1} represent the PPR concentration and the rate constant for the radical–radical reaction of PPRs, respectively. Integration of Eq. (2) leads to Eq. (3) where $[RM^{\cdot}] = [RM^{\cdot}]_s$ at $t = 0$:

$$\frac{[RM^{\cdot}]_s}{[PM^{\cdot}]} = k_{t1}[RM^{\cdot}]_s t + 1 \quad (3)$$

The second-order plot (Fig. 3(b)) is not linear, indicating that Eq. (3) does not correctly account for the decay curve observed. As reported in our previous paper [15], the PPR from MMAD and the *tert*-butoxy radical undergoes

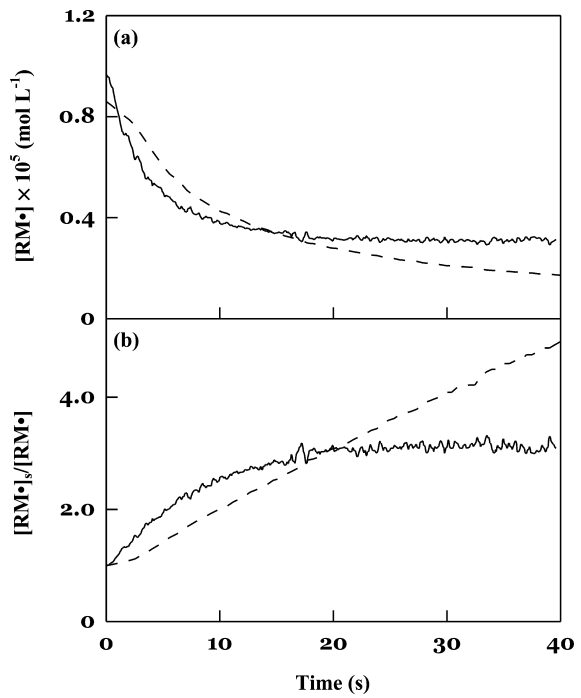

Fig. 3. Decay curves (a) and second-order plots (b) for the reaction of **1** in benzene: [MMAD] = 1.0 mol L^{-1} and $R_i = 2.1 \times 10^{-5}$ mol L^{-1} s^{-1} at 10 °C (– – –) and at 30 °C (—).

β-fragmentation to expel the 2-carbomethoxy-2-propyl radical. It was thus considered that β-fragmentation of the PPR may affect the radical decay causing deviation from second order kinetics. If PPRs were also lost by β-fragmentation, the second-order plot would exhibit upward curvature at low radical concentration. However, simulations involving Eqs. (4)–(7) (discussed in detail later) confirmed that if the addition reaction of the expelled radical to MMAD (regenerating PPR) is also considered, downward curvature as that observed experimentally may be obtained. A temperature decrease is expected to result in a decrease in the rate of fragmentation (a unimolecular reaction) relative to the rate of radical–radical reaction (a bimolecular reaction) because the activation energy for fragmentation is generally higher than for a bimolecular reaction [4,18]. In order to suppress β-fragmentation and simplify the kinetic analysis of the after-effect, the temperature was reduced to 10 °C. The second-order plot at 10 °C (Fig. 3(b)) shows much better linearity than at 30 °C in spite of the similar steady-state concentrations of **1** (see $[RM^{\cdot}]$ at $t = 0$ in Fig. 3(a)), indicating that the effect of β-fragmentation was effectively suppressed. The slope of the second-order plot ($0.10\ s^{-1}$) and the concentration of **1** at the steady-state (8.6×10^{-6} mol L^{-1}) give $k_{t1} = 1.2 \times 10^4$ L $mol^{-1}\ s^{-1}$ at 10 °C. The value of k_{t1} at 30 °C was estimated to be 1.7×10^4 L $mol^{-1}\ s^{-1}$ based on the activation energy, 8.1 kJ mol^{-1} for bimolecular termination of the propagating radical of M(DM)EA [3]. This is approximately one order of magnitude higher than k_{t1} for M(TE)EA with the 2,2,4-trimethyl-2-pentyl radical at 60 °C [13] as a result of greater steric congestion around the radical center due to the three carbethoxy groups and the bulky 2,4,4-trimethyl-2-pentyl group.

The experimental data and simulations assuming second order kinetics using Eq. (2) ($k_\beta = 0$) with the estimated k_{t1} value are shown in Fig. 4. The PPR concentration of the experimental data reached a 'second steady-state' during the after-effect, at 3.3×10^{-6} mol L^{-1}, and remain at this level even after as long as 840 s (the EPR spectrum shown in Fig. 2(b) was recorded during the second steady-state). On the other hand, the simulated PPR concentration decreases more rapidly to lower concentration. The relatively high PPR concentration at the second steady-state may indicate regeneration of the PPR by addition of expelled radicals because the thermolysis of MAIB at 30 °C is negligible ($k_d = 5.2 \times 10^{-8}\ s^{-1}$) based on the time scale of the after-effect [19]. In effect, radical–radical reaction of PPR must now compete with fragmentation, and due to the regeneration step, this leads to a lower rate of net loss of PPR. The difference in the basic shape of the simulated (assuming no fragmentation) and experimental decay curves (Fig. 4) is similar to the difference between the experimental curves at 10 and 30 °C (Fig. 3(a)), indicating that the effect of β-fragmentation is much smaller at 10 °C, and may indeed be negligible.

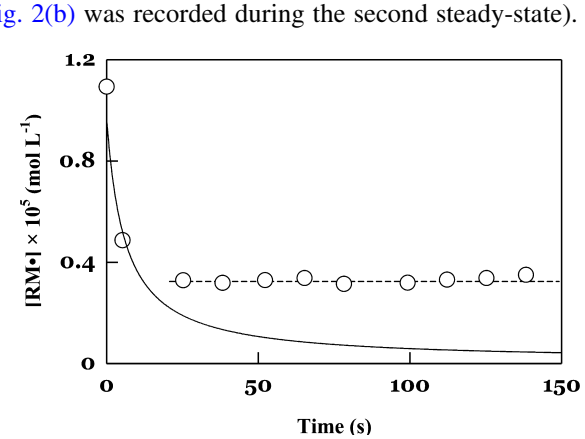

Fig. 4. Decay curve of *1* at 30 °C in benzene (○) and simulated curve (Eq. (2)) without β-fragmentation (—): [MMAD] = 1.0 mol L^{-1} and [MAIB] = 0.28 mol L^{-1}; $k_{t1} = 1.7 \times 10^4$ L $mol^{-1}\ s^{-1}$.

3.1.2. Effect of initiator

In order to gather further evidence that PPR is regenerated by addition of expelled radicals to MMAD and that this affects the kinetic analysis, the reaction of MMAD with the 2,4,4-trimethyl-2-pentyl radical from ATMP was investigated. In this system, the PPR generated from PRI (**2**) is different from **1** formed by addition of the expelled radical from **2** to MMAD, and it is expected that **1** and **2** exhibit different reactivities (Scheme 2). Fig. 5 shows apparent values of the rate constant for radical–radical reaction of PPRs (k_{t1}'), calculated from the instantaneous slopes of the second-order plots, versus $[RM^{\cdot}]$ at different initiator concentrations for the MAIB/MMAD and the ATMP/MMAD systems. In the absence of generation of PPR by addition to MMAD of the expelled radical, k_{t1}' would be independent of initiator concentration (i.e. independent of $[RM^{\cdot}]_s$) at any given value of $[RM^{\cdot}]$, even if β-fragmentation occurs. In the MAIB/MMAD system, k_{t1}' at a given $[RM^{\cdot}]$ is independent of the initiator concentration. However, in the ATMP/MMAD system, the dependence of k_{t1}' on $[RM^{\cdot}]$ is a function of the ATMP concentration, and the $RM^{\cdot}$ would consist of species **1** and **2**. The relative amounts of **1** and **2** would change during the after-effect as a result of fragmentations followed by addition of expelled radicals to MMAD. [**2**] ≫ [**1**] at the beginning of the after-effect, but the molar fraction of **1**

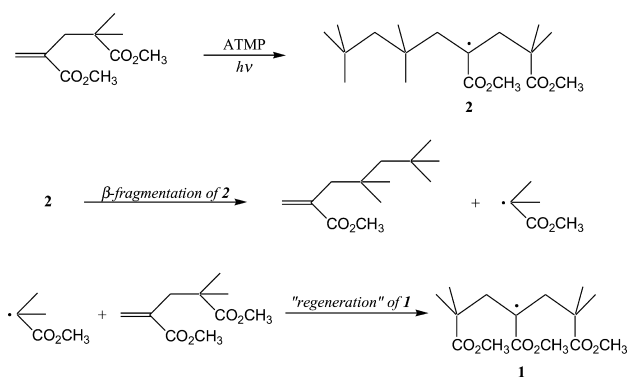

Scheme 2.

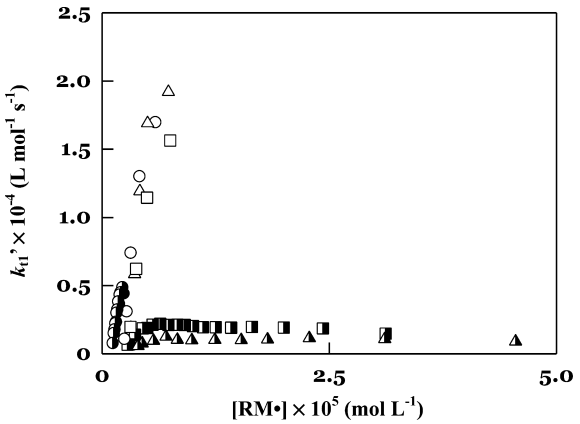

Fig. 5. Apparent values of k_{t1} at different initiator concentrations in benzene at 30 °C: [MMAD] = 1.0 mol L^{-1}: [ATMP] = 0.005 mol L^{-1} and [RM$^{\cdot}$]$_s$ = 2.42 × 10^{-6} mol L^{-1} (◑), [ATMP] = 0.010 mol L^{-1} and [RM$^{\cdot}$]$_s$ = 3.48 × 10^{-5} mol L^{-1} (◨), [ATMP] = 0.050 mol L^{-1} and [RM$^{\cdot}$]$_s$ = 5.62 × 10^{-5} mol L^{-1} (▲), [MAIB] = 0.028 mol L^{-1} and [RM$^{\cdot}$]$_s$ = 7.59 × 10^{-6} mol L^{-1} (○), [MAIB] = 0.057 mol L^{-1} and [RM$^{\cdot}$]$_s$ = 9.86 × 10^{-6} mol L^{-1} (□), and [MAIB] = 0.28 mol L^{-1} and [RM$^{\cdot}$]$_s$ = 9.74 × 10^{-6} mol L^{-1} (△).

relative to **2** gradually increases with time since no 2,4,4-trimethyl-2-pentyl radicals are now supplied by the decomposition of initiator. It follows that for any given [PPR] during the after-effect in two experiments with different [ATMP], the molar fractions of **1** and **2** will be different, and therefore the values of k_{t1}' will also be different. This explains why the MAIB initiated system gives values of k_{t1}' that are independent of the initiator concentration, unlike the ATMP initiated system (Fig. 5). The dependence of k_{t1}' on [RM$^{\cdot}$] in the case of the ATMP initiated system is complicated. The dependence is a result of the combined effect of [**1**]:[**2**], the values of the different k_β of the system, and the k_{t1}' values for **1** and **2**. This situation will be addressed in detail in a later publication.

3.2. Estimation of k_{t2}/k_{M1}

The kinetic equations based on all expected reactions are:

$$\frac{d[I]}{dt} = -k_d[I] \quad (4)$$

$$\frac{d[M]}{dt} = k_\beta[RM^{\cdot}] - k_{M1}[R^{\cdot}][M] \quad (5)$$

$$\frac{d[RM^{\cdot}]}{dt} = k_{M1}[R^{\cdot}][M] - k_{t1}[RM^{\cdot}]^2 - k_{t2}[R^{\cdot}][RM^{\cdot}] - k_\beta[RM^{\cdot}] \quad (6)$$

$$\frac{d[R^{\cdot}]}{dt} = 2k_d f[I] + k_\beta[RM^{\cdot}] - k_{M1}[R^{\cdot}][M] - k_{t2}[R^{\cdot}][RM^{\cdot}] - k_{t3}[R^{\cdot}]^2 \quad (7)$$

At the steady-state, d[RM$^{\cdot}$]/dt (Eq. (6)) and d[R$^{\cdot}$]/dt (Eq. (7)) are both equal to zero. Addition of Eqs. (6) and (7), and subtraction of Eq. (6) from Eq. (7) give Eqs. (8) and (9), respectively, and thus Eq. (10) can be derived.

$$2k_d f[I] - k_{t1}[RM^{\cdot}]^2 - k_{t3}[R^{\cdot}]^2 - 2k_{t2}[R^{\cdot}][RM^{\cdot}] = 0 \quad (8)$$

$$2k_d f[I] + k_{t1}[RM^{\cdot}]^2 - k_{t3}[R^{\cdot}]^2 + 2k_\beta[RM^{\cdot}] - 2k_{M1}[R^{\cdot}][M] = 0 \quad (9)$$

$$\frac{k_{t2}}{k_{M1}} = \frac{2k_d f[I] - k_{t1}[RM^{\cdot}]^2 - k_{t3}[R^{\cdot}]^2}{2k_d f[I] + k_{t1}[RM^{\cdot}]^2 + 2k_\beta[RM^{\cdot}] - k_{t3}[R^{\cdot}]^2} \times \frac{[M]}{[RM^{\cdot}]} \quad (10)$$

The value of k_{t3} for the 2-carbomethoxy-2-propyl radical in acetonitrile at 30 °C was obtained from the Arrhenius parameters reported by Sobek et al. $k_{t3} = 5.5 \times 10^9$ L × mol^{-1} s^{-1} [20]. However at 30 °C, the diffusion limit was predicted to be slightly lower than the chemically controlled rate constant [20]. Therefore, the data at low MMAD concentration (0.25 mol L^{-1}) have been selected for further analysis in order to be able to ignore a possible decrease in k_{t3} due to the viscosity increasing with the MMAD concentration. In order to determine k_{t2}/k_{M1} from Eq. (10), values of k_β and [R$^{\cdot}$] (at the steady-state) are required. It was tentatively assumed that the contribution of the term $k_{t3}[R^{\cdot}]^2$ was negligible, and an arbitrary k_β value was substituted into Eq. (10) for calculation of a tentative k_{t2}/k_{M1} value using $k_{t1} = 1.7 \times 10^4$ L mol^{-1} s^{-1} and $k_d f = 3.8 \times 10^{-5}$ × s^{-1}. Using this tentative k_{t2}/k_{M1} value, a new k_β value was obtained by computer simulations and curve fitting of the after-effect as described in detail below. This new k_β value and simulated [R$^{\cdot}$] at the steady-state were then substituted into Eq. (10), and this iterative procedure was continued until the k_{t2}/k_{M1} values converged, resulting in $k_{t2}/k_{M1} = 5.2 \times 10^4$ and [R$^{\cdot}$] = 4.2 × 10^{-8} mol L^{-1}.

3.3. Optimization of absolute rate constants

The rate constants k_{M1}, k_{t2} and k_β were estimated by computer simulations and parameter optimizations of the pre-effect and the after-effect based on Eqs. (4)–(7), using the already estimated values of k_{t2}/k_{M1} and k_{t1}. The change in the PPR concentration during the after-effect arising from β-fragmentation and regeneration of PPR is more significant than during the pre-effect, because generation of PRI from initiator photolysis does not occur during the after-effect. Consequently, the pre-effect was relatively insensitive to the value of k_β, and thus the optimum k_β value was obtained from simulations and curve fitting of the after-effect only. The optimum k_{M1} value was obtained from both the pre-effect and the after-effect. When optimizing for the k_{M1} value during the pre-effect, k_β estimated from the after-effect was used. The optimizations using the pre-effect and the after-effect data resulted in very similar values of k_{M1} and k_{t2}. The absolute values of k_{M1}, k_{t2} and k_β are listed in Table 1. Fig. 6 illustrates the agreement obtained between

Table 1
Optimized rate constants: [MMAD] = 0.25 mol L^{-1} and [MAIB] = 0.28 mol L^{-1} in benzene at 30 °C

$[RM^{\cdot}]_s$ (mol L^{-1})	k_{M1} (L mol^{-1} s^{-1})[a]	k_β (s^{-1})	k_{t2} (L mol^{-1} s^{-1})[b]	k_{t1} (L mol^{-1} s^{-1})
4.37×10^{-6}	3.5×10^{2}	6.2×10^{-2}	1.8×10^{7}	1.7×10^{4}

[a] Average value from pre-effect and after-effect.
[b] Calculated from k_{t2}/k_{M1} and k_{M1}.

experiment and simulations for [MMAD] = 0.25 mol L^{-1} and [MAIB] = 0.28 mol L^{-1} at 30 °C.

The value of k_{M1} (3.5×10^2 L mol^{-1} s^{-1}) is small as the addition rate constant of a small radical to a double bond. Zytowski et al. determined the rate constant for addition of the 2-carbomethoxy-2-propyl radical to MMA by time-resolved EPR spectroscopy to be 3.71×10^3 L mol^{-1} s^{-1} at 24 °C [21]. The addition rate constant to MMAD obtained in this study being smaller than for MMA by one order of magnitude is consistent with the presence of the bulky α-substituent of MMAD. We previously estimated the addition rate constants of the methyl radical and the *tert*-butoxy radical to MMAD by the nitroxide trapping method to be close to 6×10^5 and 9×10^4 L mol^{-1} s^{-1} at 60 °C, respectively [15], i.e. considerably higher than for the 2-carbomethoxy-2-propyl radical. For highly reactive radicals such as the *tert*-butoxy radical and the methyl radical, addition reactions have an early transition state, whereas in the case of less reactive and resonance stabilized free radicals, there is a late transition state [22]. Polar factors are expected to mainly govern the addition rate constant for highly reactive radicals, while resonance and steric factors also affect the reactivities in the case of less reactive radicals such as propagating radicals [22].

The value of k_β (6.2×10^{-2} s^{-1}) is greater than the rate constant of β-fragmentation for MMEA at 30 °C by more than factor of ten, calculated from the Arrhenius parameters reported by Kobatake et al. to be 4.4×10^{-3} s^{-1} [4]. This difference can be attributed to greater internal strain of the adduct radical from MMAD than the propagating radical of MMEA, and the increased stability of the tertiary carbon-centered radical expelled from the adduct radical of MMAD compared with the primary carbon-centered radical in the case of MMEA. It is deduced that not only termination but also β-fragmentation of the adduct radical may compete with propagation, and the favorable balance among propagation, termination and β-fragmentation characterizes the homopolymerizability of α-(substituted methyl)acrylates including non-polymerizable MMAD and polymerizable MMEA.

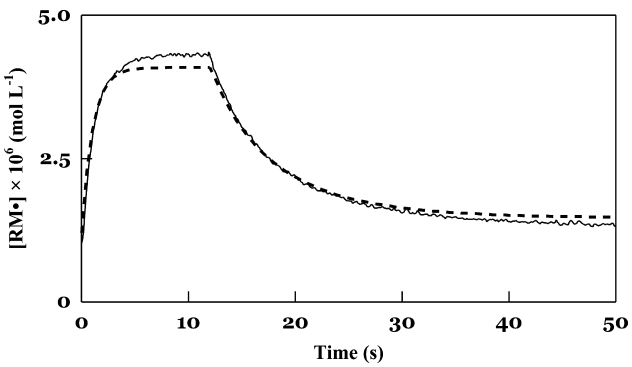

Fig. 6. Experimental (—) and simulated (– –) PPR concentration during pre-effect, steady-state and after-effect: [MMAD] = 0.25 mol L^{-1} and [MAIB] = 0.28 mol L^{-1} in benzene at 30 °C. EPR data corresponding to two separate measurements of the pre-effect (including the steady-state) and the after-effect have been combined. The average values of k_{M1} and k_{t2} from the pre-effect and the after-effect were used to simulate the entire concentration profile.

3.4. Lifetime of *1*

The expected lifetimes of **1** when considering radical–radical reaction (t_{t1}) and β-fragmentation (t_β) as the modes of radical loss separately were calculated from Eqs. (11) and (12), respectively, and are plotted versus PPR concentration in Fig. 7.

$$t_{t1} = \frac{[RM^{\cdot}]}{R_{t1}} = \frac{1}{k_{t1}[RM^{\cdot}]} \tag{11}$$

$$t_\beta = \frac{[RM^{\cdot}]}{R_\beta} = \frac{1}{k_\beta} \tag{12}$$

where R_{t1} and R_β represent the rates of consumption of PPR by radical–radical reaction and β-fragmentation, respectively. It is clear from Fig. 7 that radical–radical reaction and β-fragmentation can compete under these experimental conditions.

The magnitude of k_{t2} falls in the range between k_{t1} and k_{t3}, which is reasonable considering the level of steric congestion of the radical centers: k_{t1} is the rate constant for radical–radical reaction of the sterically hindered **1**, k_{t2} is for **1** and the 2-carbomethoxy-2-propyl radical, and k_{t3} is for

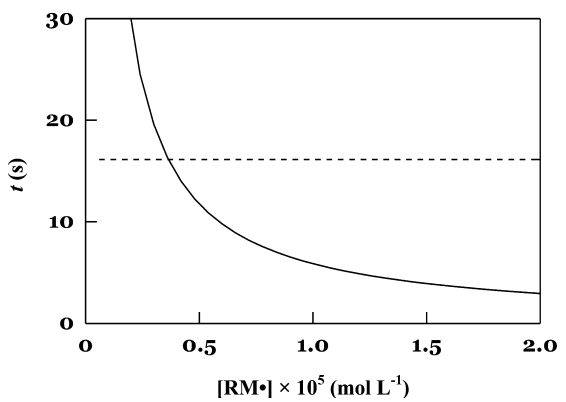

Fig. 7. Lifetime of **1** consumed by radical–radical reaction ($k_{t1} = 1.7 \times 10^4$ L mol^{-1} s^{-1}) (—) and by β-fragmentation ($k_\beta = 6.2 \times 10^{-2}$ × s^{-1}) (– –).

radical–radical reaction of 2-carbomethoxy-2-propyl radicals.

$$k_{t1} : k_{t2} : k_{t3} = 1 : 10^3 : 10^5$$

4. Conclusions

The PPR generated from MMAD and MAIB was directly detected and quantified, and the radical concentration profiles during the pre-effect, the steady-state and the after-effect were obtained by EPR spectroscopy. All rate constants for the formation and further reactions of the PPR in this system were evaluated by kinetic analysis combined with computer modeling and simulations involving parameter optimizations of the pre-effect and the after-effect. The rate constants for addition and β-fragmentation were influenced by the steric hindrance of the α-substituent of MMAD and the adduct radical. The rate constants for three types radical–radical reaction, PRI–PRI, PRI–PPR, and PPR–PPR, decrease markedly with increasing steric congestion around the radical centers. The methodology developed in this study is applicable for systems where the PPR is symmetrical, i.e. the initiating radical is the same as the expelled radical.

References

[1] Yamada B, Kobatake S. Prog Polym Sci 1994;19:1089.
[2] Yamada B, Westmoreland DG, Kobatake S, Konosu O. Prog Polym Sci 1999;24:565.
[3] Kobatake S, Yamada B. Macromolecules 1995;28:4047.
[4] Kobatake S, Yamada B. J Polym Sci Part A: Polym Chem 1996;34:95.
[5] Harada T, Zetterlund PB, Yamada B. J Polym Sci Part A: Polym Chem; in press.
[6] Sato T, Inui S, Tanaka H. J Polym Sci Part A: Polym Chem 1987;25:637.
[7] Tanaka H, Sakai K, Sato T, Ota T. Macromolecules 1988;21:3534.
[8] Kuwae Y, Kamachi M. Bull Chem Soc Jpn 1989;62:2474.
[9] Tanaka H, Miyake H, Ota T. J Macromol Sci Chem 1984;A21:1523.
[10] Sato T, Morino K, Tanaka H, Ota T. Eur Polym J 1990;26:1279.
[11] Moad CL, Moad G, Rizzardo E, Thang SH. Macromolecules 1996;29:7717.
[12] Tanaka H, Kawai H, Sato T. J Polym Sci Part A: Polym Chem 1989;27:1741.
[13] Yamada B, Kobatake S, Konosu O. Macromol Chem Phys 1996;197:901.
[14] Odian G. Principles of Polymerization, 3rd ed. New York: Wiley; 1991. Chapter 3.
[15] Sato E, Zetterlund PB, Yamada B, Jenkins ID, Busfield WK. Polym Int; in press.
[16] Abbey KJ, Carlson GM, Masola MJ, Zander RA. J Polym Sci Part A: Polym Chem 1993;31:3417.
[17] Bizilj S, Kelly DP, Serelis AK, Solomon DH, White KE. Aust J Chem 1985;38:1657.
[18] Fossey J, Lefort D, Sorba J. Free radicals in organic chemistry. Chichester: Wiley; 1995. Chapter 12.
[19] Dixon KW. Decomposition rates of organic free radical initiators. In: Brandrup J, Immergut EH, Grulke EA, editors. Polymer handbook, 4th ed. New York: Wiley; 1999.
[20] Sobek J, Martschke R, Fischer H. J Am Chem Soc 2001;123:2849.
[21] Zytowski T, Knuhl B, Fischer H. Helv Chim Acta 2000;83:658.
[22] Fossey J, Lefort D, Sorba J. Free radicals in organic chemistry. Chichester: Wiley; 1995. Chapter 6.